JCTC Journal of Chemical Theory and Computation

Article

pubs.acs.org/JCTC

Evaluation of Proteins' Rotational Diffusion Coefficients from Simulations of Their Free Brownian Motion in Volume-Occupied Environments

Maciej Długosz*,† and Jan M. Antosiewicz‡

†Center of New Technologies and ‡Department of Biophysics, Faculty of Physics, University of Warsaw, Żwirki i Wigury 93, Warsaw 02-089, Poland

Supporting Information

ABSTRACT: We have investigated the rotational dynamics of hen egg white lysozyme in monodisperse aqueous solutions of concentrations up to 250 mg/mL, using a rigid-body Brownian dynamics method that accurately accounts for anisotropies of diffusing objects. We have examined the validity of the free diffusion concept in the analysis of computer simulations of volume-occupied molecular solutions. We have found that, when as the only intermolecular interaction, the excluded volume effect is considered, rotational diffusion of molecules adheres to the free diffusion model. Further, we present a method based on the exact (in the case of the free diffusion) analytic forms of autocorrelation functions of particular vectors rigidly attached to diffusing objects, which allows one to obtain from results of molecular simulations the three principal rotational diffusion coefficients characterizing rotational Brownian motion of an arbitrarily shaped rigid particle for an arbitrary concentration of crowders. We have applied this approach to trajectories resulting from Brownian dynamics simulations of hen egg white lysozyme solutions. We show that the apparent anisotropy of proteins' rotational motions increases with an increasing degree of crowding. Finally, we demonstrate that even if the hydrodynamic anisotropy of molecules is neglected and molecules are simulated using their average translational and rotational diffusion coefficients, excluded volume effects still lead to their anisotropic rotational dynamics.

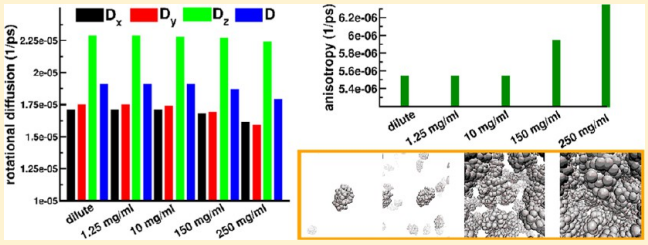

1. INTRODUCTION

Translational and rotational motions of molecules in soft condensed media, like aqueous solutions or interior of living cells, have been a subject of physical, chemical, or biological interest. Among many issues that await systematic studies using both theoretical as well as experimental approaches is the description of the effects of different interactions with cosolutes, either short-range or long-range, direct or indirect (such as mediated via the surrounding solvent hydrodynamic interactions), on the rotational dynamics of particles undergoing translational and rotational Brownian motions. Here, we are interested in rotational motions of proteins and macromolecules in general, treated as rigid bodies of arbitrary shape, when their rotations result from many very small, uncorrelated angular displacements, and thus can be described by the rotational diffusion equation.[1,2] Using monodisperse solutions of hen egg white lysozyme (HEWL, Figure 1) as model systems, we study the orientational relaxation of molecules in volume-occupied environments (or under so-called crowded conditions) by means of rigid-body Brownian dynamics simulations.[3−5] Our analysis of the simulated trajectories remains in a close relationship with theoretical interpretations of experiments devoted to study the rotational dynamics of molecules in the liquid phase.

One kind of a convenient and a powerful experimental tool in the field of studies of nanosecond and subnanosecond orientational dynamics of molecules in the condensed phase was established by time-domain spectroscopy with polarized light. The signal decays observed in these experimental techniques, when interpreted under the assumption of the

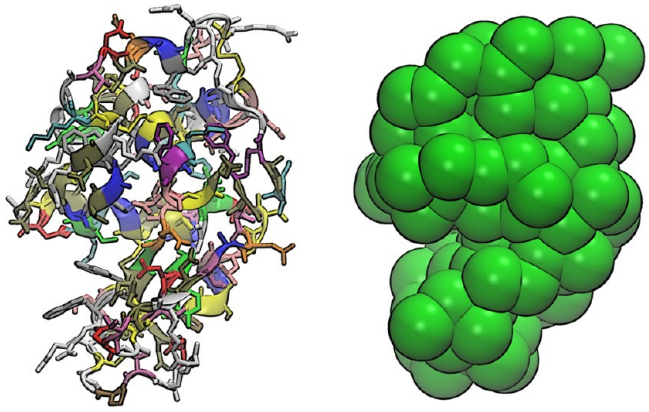

Figure 1. Atomic structure of the hen egg white lysozyme molecule, PDB ID 6LYZ[35] (left) and its bead model (right). Drawings were done using the VMD package.[36]

Received: September 27, 2013
Published: December 5, 2013

dx.doi.org/10.1021/ct4008519 | J. Chem. Theory Comput. 2014, 10, 481−491

linear response, are related to $P_2[\vec{\mu}(0)\cdot\vec{\mu}(t)]$, the second Legendre polynomial ($P_2[x] = 1/2(3x^2 - 1)$) of a two-time dipole correlation function.[6] For example, in fluorescence depolarization experiments,[7−10] the molecule is first excited by the polarized light, and subsequently, the intensities of fluorescence polarized in planes parallel ($I_{\parallel}(t)$) and perpendicular ($I_{\perp}(t)$) to the polarization plane of the exciting light are measured as a function of the time following the excitation. The polarization anisotropy function is given by

$$r(t) = \frac{I_{\parallel}(t) - I_{\perp}(t)}{I_{\parallel}(t) + 2I_{\perp}(t)} = \frac{2}{5}\langle P_2(\vec{\mu}(t)\cdot\vec{\mu}(0))\rangle \quad (1)$$

where $\vec{\mu}$ is the transition dipole. Scalar product $\vec{\mu}(0)\cdot\vec{\mu}(t)$ gives $\cos(\theta(t))$, where $\theta(t)$ is the angle between $\vec{\mu}$ at time t and itself at time 0. Averaging is performed over all molecules. Other experimental techniques such as electric birefringence and dichroism,[11] and NMR relaxation,[12] also relate observed properties of the studied system to the average of the second Legendre polynomial of the angle subtended by two successive orientations of a certain vector within a particle. On the other hand, in methods like dielectric relaxation spectroscopy, the time-dependent behavior of the electric polarization can be related to the first Legendre polynomial $P_1[\vec{\mu}(0)\cdot\vec{\mu}(t)]$ ($P_1[x] = x$).[13] Analysis of the experimental data in terms of specific $r(t)$ functions allows one to obtain diffusion coefficients characterizing rotational Brownian motions of investigated molecules because the time dependence of $r(t)$ can be predicted by solving the appropriate rotational diffusion equation.[14−20] Functions $r(t)$ expressed either using $P_1[\vec{\mu}(0)\cdot\vec{\mu}(t)]$ or $P_2[\vec{\mu}(0)\cdot\vec{\mu}(t)]$ are called rotational correlation functions (RCF).

Theoretical interpretation of the above-mentioned experiments in terms of rotational diffusion coefficients was developed under the assumption of independently rotating particles undergoing Brownian motion and therefore was strictly applicable only to dilute solutions.[11,14−16,19−25] Another important issue in the theoretical developments was the notion of the force-free rotational diffusion, i.e. diffusion that occurs in the absence of any external fields, like the external electric field, which may induce preferences for some orientations of molecules in the laboratory coordinate system (LCS). It has been shown that in the most general case of freely diffusing rigid particles of arbitrary shape, the two-time dipole correlation function, $r(t)$, is a multiexponential decay function, having up to three, in the case of $r(t) \propto \langle P_1[\vec{\mu}(0)\cdot\vec{\mu}(t)]\rangle$ or having up to five, in the case of $r(t) \propto \langle P_2[\vec{\mu}(0)\cdot\vec{\mu}(t)]\rangle$, components.[11,14−16,19,20,23−25]

Theoretical studies on rotational motions of molecules can be performed using computer simulation methods such as molecular dynamics,[26,27] Langevin dynamics,[28,29] or Brownian dynamics.[5,30−33] These techniques allow one to monitor the reorientation of certain particle-fixed vectors in the laboratory coordinate system and to evaluate their two-time RCFs. As it is presented on a few examples that are discussed below, these correlation functions are usually fit with one or two exponential terms. Exponents resulting from these fits are treated as estimates of molecular rotational diffusion coefficients and compared directly with available experimental results.

Frembgen-Kesner and Elcock[32] performed coarse-grained Brownian dynamics simulations of 11 different proteins in their folded state. Rotational dynamics of these proteins was quantified by computing separately $\langle P_1[\vec{\mu}(0)\cdot\vec{\mu}(t)]\rangle$ functions for the three vectors pointing along the principal axes of the proteins' moments of inertia. The three correlation functions were then averaged, and the resulting average curve was fit to a single-exponential function (additional exponential terms were found to be unnecessary); the time constant of this decay was interpreted as the rotational relaxation time τ_{rot}, from which the rotational diffusion coefficient was calculated directly as $D_{rot} = (1/2\tau_{rot})$.

In yet another rigid-body Brownian dynamics study from the Elcock's group,[31] the authors use a similar approach to evaluate rotational dynamics of proteins in the cytoplasm model and find it to be transiently anomalous.[34]

Mereghetti and Wade[30] performed rigid-body Brownian dynamics simulations of concentrated solutions (30−40% volume fraction) of myoglobin, hemoglobin A, and sickle cell hemoglobin S. The rotational diffusion coefficient, for each protein, was obtained by computing the time-ensemble averaged autocorrelation function of the protein orientation vectors $\vec{\mu}$, which were then fit with a single-exponential curve of the form $\langle P_1[\vec{\mu}(0)\cdot\vec{\mu}(t)]\rangle \propto Ae^{-t/\tau_{rot}}$. The rotational diffusion coefficient was obtained from the relaxation time τ_{rot} as $D^{rot} = (1/2\tau_{rot})$.

We should note at this point that the rigid-body Brownian dynamics studies described above[30,31] employed a Brownian dynamics algorithm based on average translational and rotational diffusion coefficients of molecules although all of the proteins considered by these authors exhibit some degree of hydrodynamic anisotropy.

On the other hand, Hu et al.[27] performed MD simulations of substrate-free *S*-adenosyl-L-homocysteine hydrolase and calculated decays $\langle P_2[\vec{\mu}(0)\cdot\vec{\mu}(t)]\rangle$ for each of the principal axes of the moments of inertia of the protein (represented by $\vec{\mu}$). The characteristic times were determined by fitting the resulting decays with two-exponential functions of the form: $\langle P_2[\vec{\mu}(0)\vec{\mu}(t)]\rangle = \Sigma_{i=1}^{2} a_i(\exp(-t/\tau_i) - 1)$. The calculated times τ_i were directly compared with the fluorescence anisotropy decay data.

Finally, Ravichandran et al.[26] simulated diffusion trajectories of ellipsoidal molecules immersed in the solvent containing spherical crowding molecules using MD. The dynamical behavior of the ellipsoidal molecules was monitored via calculation of decays $\langle P_1[\vec{\mu}(0)\cdot\vec{\mu}(t)]\rangle$ and $\langle P_2[\vec{\mu}(0)\cdot\vec{\mu}(t)]\rangle$ where $\vec{\mu}$ is a unitary vector colinear with the symmetry axis of the molecule. These authors noted that while the translational motion of an ellipsoid is isotropic at low density, it becomes increasingly anisotropic with density until the ratio of the parallel to the perpendicular diffusion coefficients becomes nearly equal to the value of the aspect ratio. Moreover, they noted that the first-rank (i.e., $\langle P_1[\vec{\mu}(0)\cdot\vec{\mu}(t)]\rangle$) rotational correlation function becomes nonexponential at the high density and low temperature where it also develops a slow decay, and at the highest density studied, the long-time decay of the rotational correlation function could be fit to a stretched-exponential function.[26]

Such treatment of the simulated data raises some questions. The first question regards physical meaning of the exponents resulting from fitting of single- or multiexponential functions to RCFs derived from simulations. Here we recall some published theoretical works which clearly indicate that exponents resulting from such fits are undefined functions of rotational diffusion coefficients rather than the rotational diffusion coefficients themselves. The second question concerns the applicability of the free diffusion concept in the analysis of simulations in the so-called crowded environment. We show

that when, as the only intermolecular interaction, the excluded volume effect is taken into account, the rotational diffusion of molecules satisfies requirements of the free diffusion. Moreover, we show that even if the diffusion of anisotropic molecules is simulated isotropically using effective (average) translational and rotational diffusion coefficients, excluded volume effects still lead to the anisotropic rotational dynamics of molecules. We thus suggest that using of isotropic diffusion coefficients to model arbitrarily shaped particles, particularly aspherical ones, may be inadequate. Finally, we present a method which allows one to obtain, from results of molecular simulations analyzed in terms of the $P_1[x]$ and $P_2[x]$, the three principal rotational diffusion coefficients characterizing the rotational Brownian motion of an arbitrarily shaped rigid particle for an arbitrary concentration of crowders.

While in the current work the term *crowded* corresponds exclusively to volume-occupied solutions, as we consider only steric interparticle interactions, we recognize the importance of other interactions, such as electrostatic, hydrophobic, and finally solvent-mediated hydrodynamic interactions. These are bound to influence the translational as well as rotational dynamics of molecules in dense solutions.[37−39] However, the focus of our study is on shape-related effects, for which steric interactions are of primary importance. Moreover, we do not aim in the current study at characterizing quantitatively the diffusion of HEWL under various conditions, but rather we present and validate a rigorous and physically sound method of extracting rotational diffusion parameters of particles from BD simulations. Additionally, it should be noted that, even though in principle the evaluation of hydrodynamic interactions in the system of aspherical rigid bodies is possible,[40,41] rigid-body BD simulations of geometrically detailed protein models with hydrodynamic interactions enabled are not computationally feasible at present.

2. METHODS

2.1. Rotational Brownian Motion of a Free Rigid Molecule. Diffusional translations and rotations of rigid particles of arbitrary shapes are governed by their 6 × 6 diffusion tensors, containing four 3 × 3 blocks related to the translational (tt) and rotational (rr) diffusivities and their couplings (tr, rt):[5,42]

$$\mathbf{D} = \begin{pmatrix} \mathbf{D}^{tt} & \mathbf{D}^{tr} \\ \mathbf{D}^{rt} & \mathbf{D}^{rr} \end{pmatrix} \tag{2}$$

where $\boldsymbol{D}^{rt}$ is a transpose of $\boldsymbol{D}^{tr}$. $\boldsymbol{D}^{tt}$ and $\boldsymbol{D}^{tr}$ (and hence also $\boldsymbol{D}^{rt}$) depend on the location of the origin of the particle coordinate system (PCS). Translational and rotational tensors, $\boldsymbol{D}^{tt}$ and $\boldsymbol{D}^{rr}$, are always symmetric, but the coupling block $\boldsymbol{D}^{tr}$ is symmetric only when the origin of the PCS is located at the molecule's center of diffusion (CD).[43,44] As the $\boldsymbol{D}^{rr}$ tensor is symmetric, it can be diagonalized, leading to the three eigenvalues and three orthogonal principal axes. It is often convenient to assume (as we do for the purpose of this work) that these axes, originating in the particle's CD, form the PCS. Diffusion tensors of molecules can be obtained theoretically from rigid-body hydrodynamic calculations performed for atomistically detailed molecular models.[45−47]

Following others,[5,11,12,15,16,21,26,27,30−32,48] we analyze rotations of molecules obtained from our Brownian dynamics simulations in terms of rotational correlation functions:

$$C_1(t) = \langle P_1[\vec{v}(0)\cdot\vec{v}(t)]\rangle = \langle \vec{v}(0)\cdot\vec{v}(t)\rangle \tag{3}$$

and

$$C_2(t) = \langle P_2[\vec{v}(0)\cdot\vec{v}(t)]\rangle = \left\langle \frac{3}{2}(\vec{v}(0)\cdot\vec{v}(t))^2 - \frac{1}{2} \right\rangle \tag{4}$$

where $\vec{v} = (v_1, v_2, v_3)$ is a certain unitary, molecule-fixed vector defined in the PCS, and $P_1[x]$ and $P_2[x]$ are Legendre polynomials of index 1 and 2, respectively. The symbol $\langle\rangle$ denotes an average over the choice of the initial state (i.e., the orientation in the laboratory coordinate system, LCS) of a particular molecule and over the ensemble of molecules, as we first compute RCFs for each HEWL molecule in the simulation cell and then take their average.

From the fundamental work of Favro,[14] it is known that depending on the symmetry of the particle and the orientation of $\vec{v}$ in the PCS, in case of a freely rotating rigid molecule, the $C_1(t)$ function will involve up to three relaxation times ($\tau_i^{(1)}$), i.e:

$$C_1(t) = \sum_{i=1}^{i=3} a_i^{(1)} e^{-t/\tau_i^{(1)}} \tag{5}$$

whereas the $C_2(t)$ function may involve up to five relaxation times ($\tau_i^{(2)}$):

$$C_2(t) = \sum_{i=1}^{i=5} a_i^{(2)} e^{-t/\tau_i^{(2)}} \tag{6}$$

The relaxation times in the above multiexponential decays depend on the eigenvalues of particle's $\boldsymbol{D}^{rr}$ tensor, while the amplitudes ($a_i^{(1)}$, $a_i^{(2)}$) depend on the eigenvalues of particle's $\boldsymbol{D}^{rr}$ tensor as well as on the components of $\vec{v}$ in the PCS. The general expressions for $\tau_i^{(1)}$, $\tau_i^{(2)}$, $a_i^{(1)}$, and $a_i^{(2)}$ can be found in the literature[5,14,49,50] (see also the Supporting Information). We focus on a somewhat special case, namely we will consider the three unitary vectors $\vec{v}_x$, $\vec{v}_y$, $\vec{v}_z$, that are colinear with the main axes of diffusional rotations of a rigid particle, whose components in the PCS are the following:

$$\vec{v}_x = (1, 0, 0) \qquad \vec{v}_y = (0, 1, 0) \qquad \vec{v}_z = (0, 0, 1) \tag{7}$$

Denoting eigenvalues of $\boldsymbol{D}^{rr}$ by D_x^{rr}, D_y^{rr}, and D_z^{rr} and assuming that the free diffusion concept is valid, we may write (see also the Supporting Information)

$$C_1^x(t) = \langle P_1[\vec{v}_x(0)\cdot\vec{v}_x(t)]\rangle = e^{-(3D^{rr}-D_x^{rr})\cdot t} \tag{8}$$

$$C_1^y(t) = \langle P_1[\vec{v}_y(0)\cdot\vec{v}_y(t)]\rangle = e^{-(3D^{rr}-D_y^{rr})\cdot t} \tag{9}$$

$$C_1^z(t) = \langle P_1[\vec{v}_z(0)\cdot\vec{v}_z(t)]\rangle = e^{-(3D^{rr}-D_z^{rr})\cdot t} \tag{10}$$

and

$$C_2^x(t) = \langle P_2[\vec{v}_x(0)\cdot\vec{v}_x(t)]\rangle = \frac{3}{2}e^{-6D^{rr}\cdot t}\left(\frac{2}{3}\cosh(2\Delta\cdot t) + \frac{D_x^{rr} - D^{rr}}{\Delta}\sinh(2\Delta\cdot t)\right) \tag{11}$$

dx.doi.org/10.1021/ct4008519 | J. Chem. Theory Comput. 2014, 10, 481−491

$$C_2^y(t) = \langle P_2[\vec{v}_y(0)\cdot\vec{v}_y(t)]\rangle = \frac{3}{2}e^{-6D^{rr}\cdot t}\left(\frac{2}{3}\cosh(2\Delta\cdot t) + \frac{D_y^{rr} - D^{rr}}{\Delta}\sinh(2\Delta\cdot t)\right) \quad (12)$$

$$C_2^z(t) = \langle P_2[\vec{v}_z(0)\cdot\vec{v}_z(t)]\rangle = \frac{3}{2}e^{-6D^{rr}\cdot t}\left(\frac{2}{3}\cosh(2\Delta\cdot t) + \frac{D_z^{rr} - D^{rr}}{\Delta}\sinh(2\Delta\cdot t)\right) \quad (13)$$

where D^{rr} is the average rotational diffusion coefficient (or the rotational diffusion coefficient of the equivalent sphere) defined as

$$D^{rr} = \frac{1}{3}\mathrm{Tr}(\mathbf{D}^{rr}) = \frac{1}{3}(D_x^{rr} + D_y^{rr} + D_z^{rr}) \quad (14)$$

and Δ measures the particle's hydrodynamic anisotropy:

$$\Delta = \sqrt{\frac{1}{2}((D_x^{rr} - D_y^{rr})^2 + (D_x^{rr} - D_z^{rr})^2 + (D_y^{rr} - D_z^{rr})^2)} \quad (15)$$

We observe that functions $C_2^x(t)$, $C_2^y(t)$, and $C_2^z(t)$ can be linearly combined, which leads to

$$\bar{C}_2(t) = \frac{1}{3}(C_2^x(t) + C_2^y(t) + C_2^z(t)) = e^{-6D^{rr}\cdot t}\cosh(2\Delta\cdot t) \quad (16)$$

or

$$\bar{C}_2(t) = \frac{1}{2}e^{-(6D^{rr}-2\Delta)\cdot t} + \frac{1}{2}e^{-(6D^{rr}+2\Delta)\cdot t} \quad (17)$$

In case of a hydrodynamically isotropic particle (sphere), for which $D_x^{rr} = D_y^{rr} = D_z^{rr} = D^{rr}$, the above correlation functions take much simpler form:

$$C_1^x(t) = C_1^y(t) = C_1^z(t) = e^{-2D^{rr}\cdot t} \quad (18)$$

and

$$\bar{C}_2(t) = C_2^x(t) = C_2^y(t) = C_2^z(t) = e^{-6D^{rr}\cdot t} \quad (19)$$

However, as biomolecules are rarely isotropic, their rotational dynamics should be investigated using eqs 8−13. In the current work, we analyze HEWL's rotational diffusion in terms of the three $C_1^{i=x,y,z}(t)$ functions given with eqs 8−10 and the $\bar{C}_2(t)$ function given with eq 17. We fit the functions $C_1^{i=x,y,z}(t)$ (eqs 8−10) to $\langle P_1[\vec{v}_{i=x,y,z}(0)\cdot\vec{v}_{i=x,y,z}(t)]\rangle$ decay curves (eq 3) that we derive from the simulated BD trajectories of HEWL systems, then we combine the resulting terms $3D^{rr} - D_{i=x,y,z}^{rr}$ to obtain the anisotropy parameter Δ (eq 15). Having the value of Δ, we fit $\bar{C}_2(t)$ (eq 17) to $1/3(\langle P_2[\vec{v}_x(0)\cdot\vec{v}_x(t)]\rangle + \langle P_2[\vec{v}_y(0)\cdot\vec{v}_y(t)]\rangle + \langle P_2[\vec{v}_z(0)\cdot\vec{v}_z(t)]\rangle)$ decays (eq 4) as a function of only a single parameter, namely D^{rr}—the average rotational diffusion coefficient. We note that both Δ and D^{rr} values could in principle be determined by fitting of the two-parameter $\bar{C}_2(t)$ function. However, our attempts to derive both parameters from such fits resulted in overestimated values of Δ as a consequence of the fact that in the studied cases the value of the $(\Delta/3D)$ ratio (see eq 17) is rather small, roughly of 0.1, which makes reliable nonlinear fitting of the two-parameter double-exponential functions rather difficult. The benefit of the more complicated procedure (involving both $P_1[x]$ and $P_2[x]$ polynomials) which we apply in our work is that we are not only able to determine the values of D^{rr} and Δ but also the three eigenvalues of the $\mathbf{D}^{rr}$ tensor, i.e. D_x^{rr}, D_y^{rr}, D_z^{rr}.

All analyses of RCFs that we describe further were performed from time equal zero up to time for which the magnitude of a particular RCF drops $2e$ times (where e is Euler's number).

2.2. Rigid-Body Brownian Dynamics Simulations.

2.2.1. Rigid-Body Brownian Dynamics Algorithm. The propagation scheme for a rigid body of an arbitrary shape can be written in its PCS as[3−5]

$$\Delta\vec{x}(\Delta t) = \frac{\Delta t}{k_B T}\mathbf{D}\vec{M} + \vec{R}(\Delta t) \quad (20)$$

where $\mathbf{D}$ is the precomputed 6×6 diffusion tensor of the molecule (eq 2) evaluated in the PCS, Δt is the time step, $\vec{x}$ is the vector describing the position of the CD $(\vec{r})$ and orientation $(\vec{\phi})$ of the molecule, $\vec{x} = (\vec{r}, \vec{\phi})^T$, in the PCS. $\vec{M}$ is the generalized force resulting, for example, from interactions with other molecules or external fields and having two components: the total force $(\vec{F})$ and the total torque $(\vec{T})$ referred to the CD, $\vec{M} = (\vec{F}, \vec{T})^T$. $\vec{R}(\Delta t)$ is a random displacement vector arising from the Brownian noise, with zero mean, and the variance-covariance given with

$$\langle\vec{R}(\Delta t)\cdot(\vec{R}(\Delta t))^T\rangle = 2\mathbf{D}\Delta t \quad (21)$$

Random displacements of the particle can be computed via the Cholesky decomposition of its diffusion tensor.[3] The Brownian dynamics trajectory of an object in the laboratory frame can be obtained by applying at each BD simulation step transformations—translations and rotations[5]—between the PCS and the laboratory coordinate frame.

2.2.2. Hydrodynamic Model of the HEWL Molecule. The rigid-body diffusion tensor of a single HEWL molecule was evaluated using the approach described previously.[51,52] We created a bead representation of the HEWL molecule by placing spherical frictional elements at centers of coordinates of the non-hydrogen atoms of amino acids. Each element was assigned a radius computed as the mean maximal distance of any atom of a given amino acid, from the center of its bead, increased by the radius of a water molecule (i.e., 1.4 Å). Resulting hydrodynamic model of the HEWL molecule consisted of 129 beads with radii of 4.24 Å (Figure 1). Diffusion tensor of such a bead model was then evaluated using well-established methods[45−47] (Table 1) with the temperature set to 298 K and the solvent viscosity set to 0.01 P.

2.2.3. Excluded Volume Interactions. We use the coarse-grained representation of HEWL introduced above also to model excluded volume interactions between molecules. These are evaluated as the negative gradient of the standard attractive/

Table 1. Rotational Diffusion Parameters of the Isolated HEWL Molecule Derived from Its X-ray Structure (PDB ID 6LYZ[35]) Using Rigid-Body Hydrodynamic Modeling[a]

D_x^{rr} (10^{-6} 1/ps)	D_y^{rr} (10^{-6} 1/ps)	D_z^{rr} (10^{-6} 1/ps)	$D^{rr} = {}^1/_3\mathrm{Tr}(\mathbf{D}^{rr})$ (10^{-6} 1/ps)	Δ (10^{-6} 1/ps)
16.9	17.2	22.5	18.9	5.5

[a]See text for details.

dx.doi.org/10.1021/ct4008519 | J. Chem. Theory Comput. 2014, 10, 481−491

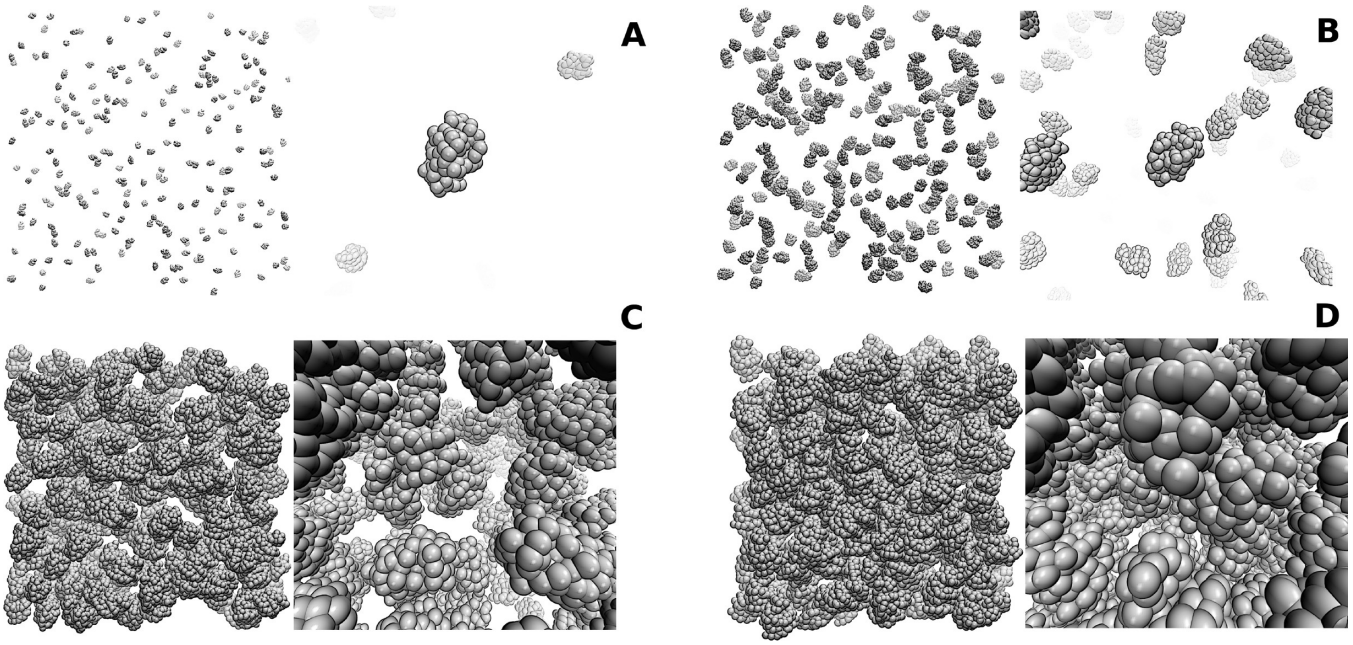

Figure 2. Snapshots of monodisperse HEWL solutions taken from BD simulations. Occupied volume fractions for hydrodynamically equivalent spherical molecules are given within parentheses: (A) density 1.25 mg/mL (0.1%); (B) density 10 mg/mL (1%); (C) density 150 mg/mL (16%); (D) density 250 mg/mL (27%). Drawings were done using the VMD package.[36]

repulsive, 6/12 Lennard-Jones potential, which for a pair of beads i and j belonging to different HEWL molecules takes the following form:

$$V^{ij} = 4\varepsilon\left(\left(\frac{2\sigma}{r_{ij}}\right)^{12} - \left(\frac{2\sigma}{r_{ij}}\right)^{6}\right) \tag{22}$$

where the σ radius is set to 4.24 Å and the well depth ε is set to kT. In our simulations the interbead cutoff of $2^{1/6}(2\sigma)$ was applied during evaluation of Lennard-Jones interactions, thus effectively only the short-range repulsion between beads of different HEWL molecules was taken into account.

2.2.4. Simulation Setup. All simulations were performed using the *BD_BOX* package[53] modified to allow for rigid-body Brownian dynamics simulations.[54] We created four HEWL systems (Figure 2). Each system consisted of 220 HEWL molecules, that, at the beginning, were positioned and oriented randomly in a cubic cell. We considered four densities of HEWL molecules: 1.25, 10, 150, and 250 mg/mL and varied the volume of the simulation cell from 1612 Å × 1612 Å × 1612 Å to 275 Å × 275 Å × 275 Å, accordingly. For the most dense system an additional BD simulation was performed, with HEWL molecules described with isotropic diffusion tensors of equivalent spheres but with intermolecular interactions considered with the full geometric detail. All systems were simulated under periodic boundary conditions that were realized via the minimum image convention. We performed also BD simulations of a single HEWL molecule that correspond to the infinite dilution limit. Temperature was set to 298 K. A single 70 μs BD trajectory was generated for each one of the investigated cases; generation of each trajectory was preceded by an equilibration stage of duration of 1.5 μs during which the simulated systems were allowed to relax from their initial states. Simulation time step (Δt in eq 20) was set to 0.75 ps. Snapshots were collected from BD trajectories every 100 steps.

Even though the time step that we use in BD simulations is relatively small and short-range repulsive forces between diffusing objects are evaluated, a small fraction of simulation steps may still result in nonphysical overlaps between molecules, due to the random term which is present in the motions equations (eq 20). We avoid such situations. After the BD step is made we check the resulting configuration of molecules in the simulated system for possible overlaps and if they are detected, all molecules are brought back to their initial positions and the BD step is attempted with different random vectors until there are no overlaps in the system. The total fraction of rejected BD steps depends on the concentration of the simulated solution and in the studied cases ranges between 0.006% (ρ = 1.25 mg/mL) and 8% (ρ = 250 mg/mL). As only steric interactions are present in the simulated systems, all nonoverlapping configurations of proteins are equally probable and thus we do not expect any accidental bias to result from this approach. While such a procedure can be quite costly in terms of the overall time that is needed to complete the simulation, the alternatives such as for example the complete neglect of overlaps between particles[55] or iterative corrections to molecules' positions and orientations introduced after a BD step is made[31,56] may, in our opinion, artificially affect the rotational dynamics of molecules in the simulated system.

3. RESULTS

3.1. Character of HEWL's Rotational Motions under Crowded Conditions. In Figure 3 we show how the orientations of HEWL's main axes of rotational diffusion (x, y, z) evolve in time. For that we evaluate distribution functions $G_{i=x,y,z}(\theta, t)$, defined as[57]

$$G_{i=x,y,z}(\theta, t) = \langle\delta\{\theta_i(t) - \theta\}\rangle = \langle\delta\{\arccos[\vec{v}_i(0)\vec{v}_i(t)] - \theta\}\rangle \tag{23}$$

dx.doi.org/10.1021/ct4008519 | J. Chem. Theory Comput. 2014, 10, 481−491

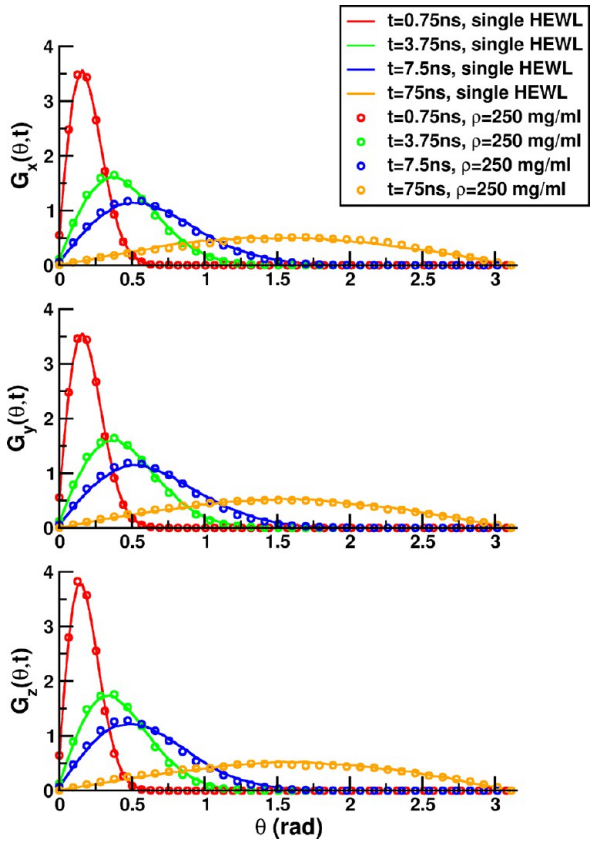

Figure 3. Orientation distributions $G_{i=x,y,z}(\theta, t)$ (eq 23) derived from BD simulations of a single HEWL molecule and a monodisperse solution of HEWL molecules of ρ = 250 mg/mL. Distributions obtained for times (t) in the range of 0.75−75 ns are depicted.

where $\theta_i(t)$ is the angle between the ith axis at time t and itself at time 0, $\vec{v}_i$ is the versor of the ith axis, $\langle\rangle$ indicates the average over the choice of the initial state of a particular molecule and over the ensemble of molecules, and

$$\delta\{\arccos(\vec{v}_i(0)\vec{v}_i(t)) - \theta\} = \begin{cases} 1 & \arccos(\vec{v}_i(0)\vec{v}_i(t)) = \theta \\ 0 & \text{elsewhere} \end{cases} \tag{24}$$

The $G_{i=x,y,z}(\theta, t)$ function defined above is the conditional probability associated with HEWL orientation at time t with respect to its orientation at time 0.

We present orientation distributions derived from BD simulations of a single HEWL molecule (infinite dilution limit) as well as distributions derived from the BD trajectory of the most concentrated HEWL solution simulated here, i.e. 250 mg/mL. $G_{i=x,y,z}(\theta, t)$ distributions are represented with histograms with particular values of θ corresponding to centers of histograms bins of width 0.01π.

According to the rigid-body BD algorithm that we apply in our simulations (eq 20), in the case of a single particle, Brownian rotations are generated via uncorrelated small angular displacements and thus the resulting rotational dynamics of the particle (in the absence of any external fields) adheres to the description provided by the free diffusion model. As a consequence, the simulation performed for the infinite dilution limit results in $G_{i=x,y,z}(\theta, t)$ distributions that are characterized by smooth curves with a single maximum and no additional structure (Figure 3). Positions of distributions' peaks shift from 0° to 90° with an increasing t. Orientation distributions derived from the simulation of the concentrated HEWL solution show similar behavior. In fact, at first glance they seem to be indistinguishable from the ones obtained in the infinite dilution limit (Figure 3). However, as the analysis described further proves, steric interactions modify the orientation distributions of HEWL on the intermediate time scale.

We first consider either very small or very large values of t. For small t the orientation distributions obtained for the dilute and the most concentrated HEWL solutions are almost identical (Figure 4, top panel). Differences are observed for

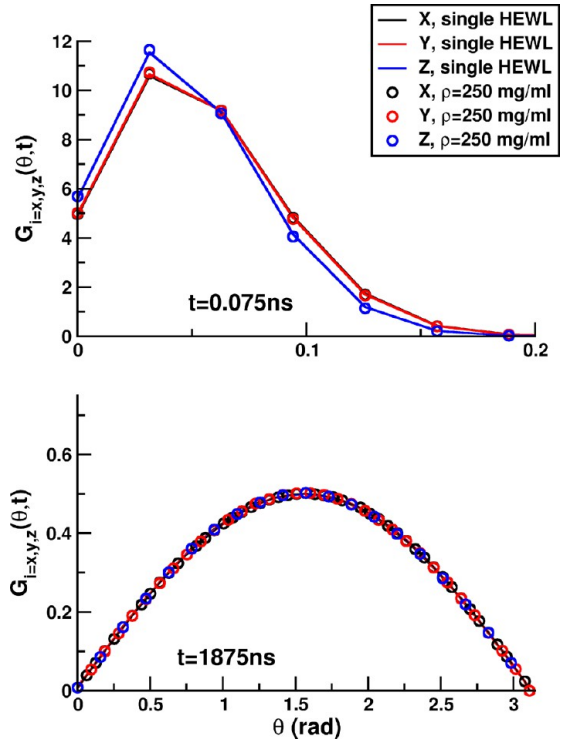

Figure 4. Orientation distributions $G_{i=x,y,z}(\theta, t)$ (eq 23) derived from BD simulations of either a single HEWL molecule or the monodisperse solution of HEWL molecules of ρ = 250 mg/mL. Distributions obtained for short (0.075 ns, top) and long (1.875 μs, bottom) times are depicted.

distributions corresponding to axes x, y, and z of the rotational diffusion tensor, which is a consequence of the fact that eigenvalues (D_x^{rr}, D_y^{rr}, D_z^{rr}) of HEWL's $\boldsymbol{D}^{rr}$ (Table 1) are not equal. In the limit of large t, distribution functions $G_{i=x,y,z}(\theta, t)$ obtained for all three rotational diffusion axes correspond to the probability density of the angle θ for the uniform distribution among $8\pi^2$ orientational states available for an arbitrarily shaped particle and are indistinguishable from each other (Figure 4, bottom panel). The above behavior is characteristic for all concentrations of HEWL solutions that we have considered.

However, the influence of steric interactions on the HEWL's rotations is visible on the intermediate time scale, as illustrated in Figures 5 and 6 where we present residuals ($\xi^{\rho}_{i=x,y,z}(\theta, t)$) computed as

$$\xi^{\rho}_{i=x,y,z}(\theta, t) = \frac{G^{\rho}_{i=x,y,z}(\theta, t) - G^{\circ}_{i=x,y,z}(\theta, t)}{G^{\circ}_{i=x,y,z}(\theta, t)} \tag{25}$$

dx.doi.org/10.1021/ct4008519 | J. Chem. Theory Comput. 2014, 10, 481−491

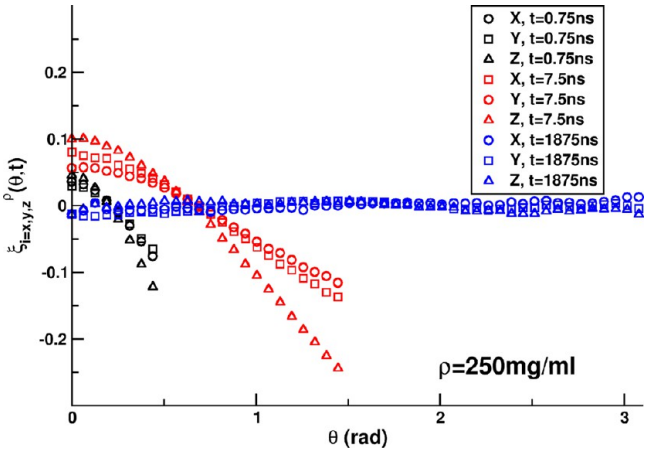

Figure 5. Comparison of orientation distributions derived from BD simulations of a single HEWL molecule and a monodisperse solution of HEWL molecules (ρ = 250 mg/mL) in terms of $\xi^{\rho}_{i=x,y,z}(\theta, t)$ functions (eq 25).

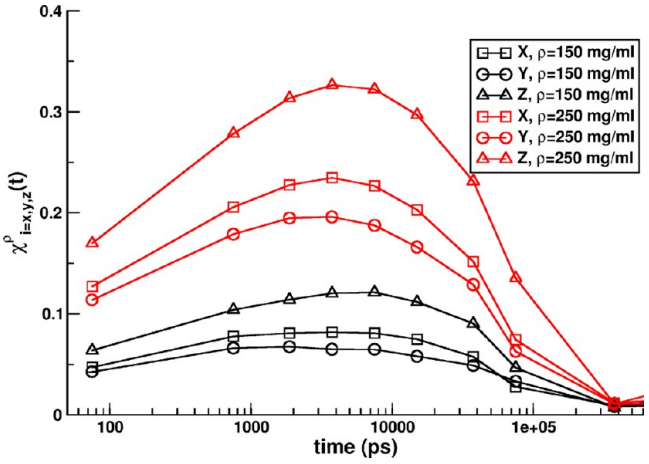

Figure 6. Comparison of orientation distributions derived from BD simulations of a single HEWL molecule and monodisperse solutions of HEWL molecules (ρ = 150, 250 mg/mL) in terms of $\chi^{\rho}_{i=x,y,z}(t)$ functions (eq 26).

where superscripts $^{\circ}$ and ρ denote the infinitely dilute and the concentrated HEWL solutions, respectively, and deviations of distributions obtained for concentrated solutions from those obtained in the case of the infinite dilution limit ($\chi^{\rho}_{i=x,y,z}(t)$):

$$\chi^{\rho}_{i=x,y,z}(t) = \sqrt{\sum_{\theta\in(0,2\pi)} (G^{\rho}_{i=x,y,z}(\theta, t) - G^{\circ}_{i=x,y,z}(\theta, t))^2} \quad (26)$$

From plots of $\xi^{\rho}_{i=x,y,z}(\theta, t)$ and $\chi^{\rho}_{i=x,y,z}(t)$, one can conclude that effects of steric interactions on HEWL's rotations are most pronounced for t of the order of a few nanoseconds. Additionally, we observe that the magnitude of these effects increases with the increasing density of the HEWL solution (Figure 6).

Our analysis of HEWL's rotations in terms of orientation distributions $G_{i=x,y,z}(\theta, t)$ (eq 23) can be summarized as follows. Collisions with other surrounding HEWL molecules restrict translational and rotational freedom of each individual HEWL molecule. It is as if a HEWL molecule would translate and rotate inside a *cavity*, although one should note that the word *cavity* is fully appropriate only for sufficiently large concentrations. The volume and shape of the cavity fluctuate with the lapse of time and the crucial point is that the time scale of these fluctuations is longer than the rotational relaxation time of an isolated HEWL molecule, as the changes in the shape and/or volume of the cavity require coordinated movements of many, randomly translating and rotating HEWL molecules that surround a particular molecule selected for observation.

On the short time scale, HEWL's rotational dynamics under crowded conditions is similar as in the infinitely dilute solution because short times implicate small angles of HEWL's rotations (and also small translations). Although the cavity on this short time scale can be considered almost rigid, the number of collisions observed between a particular molecule and molecules forming the cavity is not sufficient to influence dynamics of the observed molecule. Therefore, the overall rotational dynamics of HEWL molecules remains almost unaffected. In other words, on the short time scale some reorientations are prohibited but this does not matter because the molecules extremely rarely attempt such large reorientations. We note, that even for the most concentrated solution considered here, there is quite a lot of solvent between surfaces of the solute molecules. As an immediate consequence, distributions obtained for rotations around different principal axes of the diffusion tensor are different due to the hydrodynamic anisotropy of HEWL.

On the other hand, on the long time scale that extends beyond the characteristic time related to structural fluctuations of the simulated solution (which is longer than characteristic time of the orientational relaxation of a single HEWL molecule), all orientations of HEWL molecules in the laboratory coordinate frame are allowed. Consequently, differences in orientation distributions obtained for HEWL under dilute and under crowded conditions vanish. On a sufficiently long time scale (and what *sufficient* means depends on the concentration of HEWL molecules), orientations of the particular HEWL molecule are not restricted by steric interactions with cosolutes because the latter change their positions and orientations thus forming a continuously changing cavity. Additionally, orientation distributions obtained in the long time limit for the three principal axes of HEWL's rotational diffusion are similar, as particular values of angular displacements of different axes become equally probable for long times (the same is observed for diffusion of an isolated molecule, see Figure 4). The only characteristic influenced by an increasing concentration is the effective speed of the sampling of the orientational space available for the molecules.

However, on the intermediate time scale, it becomes important that rearrangements of the volume and shape of the above-defined cavities are slower than movements of individual HEWL molecules, and many of the angular displacements are sufficiently large to be prohibited due to steric interactions with cosolutes. Orientation distributions obtained for the infinitely dilute and for concentrated solutions of HEWL are therefore different. Moreover, steric interactions influence rotations of different HEWL's principal axes to different degrees.

The overall picture that emerges from the analysis described above is that single HEWL's rotational diffusion in the volume-occupied environment consisting of particles that undergo Brownian motions, when only excluded volume interactions between solutes are considered, can still be described as the free diffusion. Consequently, the method for obtaining effective

diffusion coefficients for crowded solutions that we employ in the current study is physically sound.

3.2. Shape Effects on HEWL's Rotational Diffusion in Volume-Occupied Environments. While some applications of BD achieve a high level of sophistication in describing molecules and their interactions,[30,31,55,56] most of the BD studies ignore the effect of molecular shapes on Brownian motions of diffusing objects. Diffusion of molecules is usually assumed to be isotropic and, instead of diffusion tensors, the average translational and rotational diffusion coefficients are used.[31,37,55,56,58,59] While such an approach may in principle be inadequate in case of biomolecules which are aspherical, studies employing BD algorithms that are based on the full diffusion tensors of molecules are rather scarce.[5,38,54,60] Here, we investigated possible consequences resulting from an application of the common rigid-body BD approaches, that neglect hydrodynamic anisotropy of diffusing objects, for the analysis of the rotational dynamics of molecules that undergo Brownian motions while influenced by steric interactions. For that, we generated two trajectories of monodisperse HEWL systems of concentrations of 250 mg/mL. We used a fully anisotropic description of HEWL molecules to simulate the first trajectory. The second trajectory was simulated with HEWL molecules assigned isotropic diffusion tensors of equivalent spherical particles. Rotational correlation functions $C_1^{i=x,y,z}(t)$ of unitary vectors assigned to the principal axes of the HEWL's rotational diffusion tensor that were derived from these trajectories (according to eq 3) are given in Figure 7.

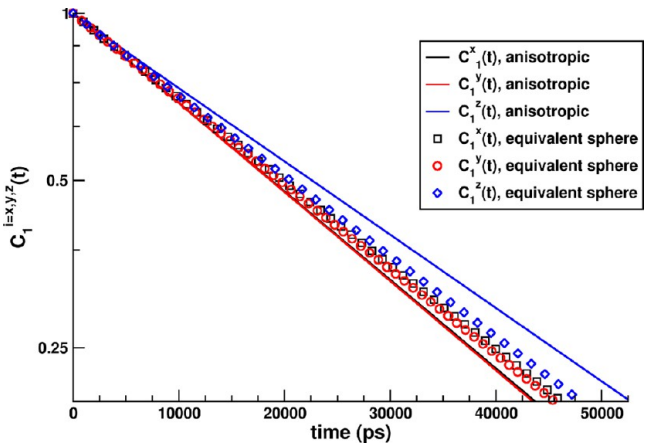

Figure 7. Rotational correlation functions $C_1^{i=x,y,z}(t)$ derived from BD simulations of monodisperse solutions of HEWL molecules, ρ = 250 mg/mL, in which HEWL molecules were assigned either a fully anisotropic diffusion tensor or an isotropic diffusion tensor of an equivalent sphere.

The three RCFs resulting from simulations of anisotropic HEWL models are clearly different, primarily due to the differences in eigenvalues of HEWL's $\boldsymbol{D}^{rr}$, D_x, D_y, and D_z. Actually, differences between $C_1^x(t)$, $C_1^y(t)$, and $C_1^z(t)$ are larger than between RCFs that can be derived in case of an infinitely dilute solution (eqs 8−10), and this will be discussed in the subsequent sections. At this point, we would like to focus rather on the three RCFs derived from the BD trajectory of the system consisting of hydrodynamically isotropic HEWL molecules. As the eigenvalues of $\boldsymbol{D}^{rr}$ are in this case identical and equal D^{rr} = (1/3)Tr ($\boldsymbol{D}^{rr}$), the three RCFs obtained for dilute HEWL solution would be also identical (eq 18). However, the three RCFs derived from the trajectory of the concentrated HEWL solution are clearly different (Figure 7), which is a consequence of HEWL's nonspherical shape and thus its anisotropic steric interactions with other (also nonspherical) solutes. Even though we have neglected the hydrodynamic anisotropy of the HEWL molecule and modeled its diffusion using an isotropic tensor, the anisotropic shape of the HEWL molecule results in its anisotropic rotational dynamics in the presence of steric interactions. It thus appears that the analysis of the rotational dynamics that employs the form of $C_1(t)$ function that is adequate only for isotropic particles (eq 18) is difficult to justify when anisotropic steric interactions between hydrodynamically isotropic solutes come into play. Analysis of $C_1^x(t)$, $C_1^y(t)$, and $C_1^z(t)$ functions separately is also problematic as the relation between time constants of the analytic decay curves that could be fit to these RCFs and the diffusion constants are not known. Moreover, it is actually unclear, what should be the form of the decay functions that could be applied to analyze the rotational dynamics resulting from the described above approach. In Table 2, we give values of the average rotational diffusion coefficients that result from fitting of monoexponential decays (eqs 18 and 19) to average rotational correlation functions $\overline{C}_1(t)$ and $\overline{C}_2(t)$, evaluated for various concentrations of HEWL molecules. We observe that the quality of fits is getting worse with an increasing concentration and that overall larger errors are observed in case of the $\overline{C}_2(t)$ function. This is understandable as the apparent anisotropy of HEWL's rotations increases with an increasing concentration (see the next section). Moreover, monoexponential fits to correlation functions obtained from the BD simulation of HEWL molecules treated as hydrodynamically isotropic particles are burden with smaller errors than corresponding fits to correlation functions obtained from the BD simulation of hydrodynamically anisotropic proteins which is a consequence of the smaller apparent anisotropy of HEWL observed in the former case (Figure 7). However, the values of average rotational diffusion coefficients derived from these two kinds of simulations are comparable.

Table 2. Average Rotational Diffusion Coefficients of HEWL Resulting from Fitting of Monoexponential Decays to Functions $\overline{C}_1(t) = {}^1/_3(C_1^x(t) + C_1^y(t) + C_1^z(t))$ and $\overline{C}_2(t) = {}^1/_3(C_2^x(t) + C_2^y(t) + C_2^z(t))$, Derived from BD Trajectories of Differently Concentrated HEWL Solutions[a]

ρ (mg/mL)	$D^{rr,b}$ (10^{-6} 1/ps)	$\delta_{RMS}{}^b$	$D^{rr,c}$ (10^{-6} 1/ps)	$\delta_{RMS}{}^c$
1.25	18.8	1.3×10^{-3}	18.7	2.0×10^{-3}
10.0	18.7	1.1×10^{-3}	18.7	2.2×10^{-3}
150.0	18.2	2.1×10^{-3}	18.3	4.6×10^{-3}
250.0	17.4	3.6×10^{-3}	17.5	9.0×10^{-3}
250.0^{isotropic}	17.3	3.0×10^{-3}	17.5	6.8×10^{-3}

[a] δ_{RMS} denotes the root mean square error of fits. Superscript isotropic indicates the simulation in which HEWL was assigned an isotropic diffusion tensor. [b] $\overline{C}_1(t) = {}^1/_3(C_1^x(t) + C_1^y(t) + C_1^z(t))$. [c] $\overline{C}_2(t) = {}^1/_3(C_2^x(t) + C_2^y(t) + C_2^z(t))$.

3.3. Evaluation of HEWL's Rotational Dynamics. Equations 8−10 give analytical forms of RCFs appropriate in case of freely diffusing particle for each one of the principal axes of the rotational diffusion tensor.[5,14,49,50] We introduce transformations $f_{i=x,y,z}$ defined as

$$f_{i=x,y,z}(\log(t)) = \log(\log((C_1^i(t))^{-1})) = \log(\log((\langle P_1[\vec{v}_i(0)\vec{v}_i(t)]\rangle)^{-1})) \quad (27)$$

which, for $C_1^{i=x,y,z}(t)$ decay curves that we derived from our BD simulations are plotted in Figure 8.

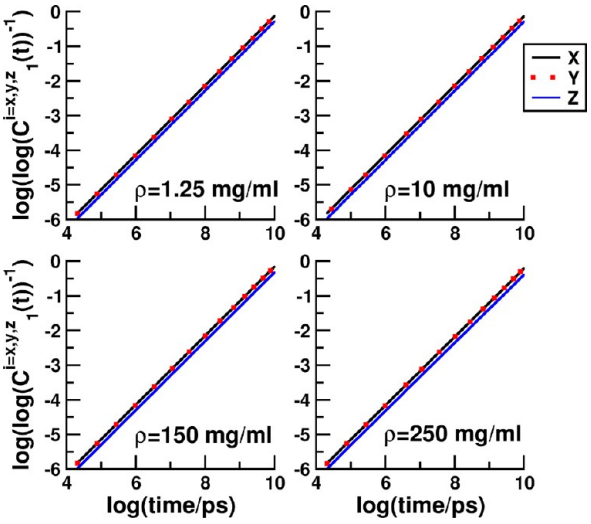

Figure 8. Plots of $\log(\log((C_1^{i=x,y,z}(t))^{-1}))$ functions derived from BD trajectories of monodisperse solutions of HEWL molecules of different densities.

In case of rotational correlation functions whose analytical forms are given by eqs 8−10, $f_{i=x,y,z}$ are linear functions of $\log(t)$:

$$f_{i=x,y,z}(\log(t)) = \log(t) + \log(3D^{rr} - D_i^{rr}) \quad (28)$$

Thus, we analyze data from Figure 8 using linear regression which allows us to ascertain, whether RCFs resulting from the simulations adhere to the monoexponential models from eqs 8−10. Moreover, based on the accuracy of linear fits to $f_{i=x,y,z}(\log(t))$, we may also exclude other models, such as stretched exponentials or multiexponential decays. In all cases presented in Figure 8 linear regression results in slope values falling between 0.99 and 1 and correlation coefficients above 0.99999, allowing us to conclude that $C_1^{i=x,y,z}(t)$ decays that we derived from BD simulations indeed adhere to monoexponential models given by eqs 8−10. Hence, the character of the rotational dynamics of HEWL in concentrated solutions is similar as in the infinite dilution limit. In addition to arguments considering orientation distributions described above, such a behavior further supports our conclusion that the rotational dynamics of HEWL in concentrated solutions can be considered as the free diffusional motion like that observed in the infinite dilution limit.

Next, we directly fit monoexponential solutions from eqs 8−11 to RCFs derived from our simulations. Resulting values of terms $3D^{rr} - D_{i=x,y,z}^{rr}$ are given in Table 3. In all of the cases, correlation coefficients between the analytic curve and the RCF were above 0.99999 and root-mean-square errors below 2.5×10^{-3}.

From the values of terms $3D^{rr} - D_{i=x,y,z}^{rr}$, it is possible to compute the anisotropy parameter, Δ (eq 15), whose values are also given in Table 3.

Table 3. Diffusional Properties of Hen Egg White Lysozyme Molecules Resulting from Fitting of Monoexponential Decays to Functions $C_1^{i=x,y,z}(t)$ Derived from BD Trajectories of Differently Concentrated Solutions of HEWL Proteins[a]

ρ (mg/mL)	$3D^{rr} - D_x^{rr}(10^{-6}$ 1/ps)	$3D^{rr} - D_y^{rr}(10^{-6}$ 1/ps)	$3D^{rr} - D_z^{rr}(10^{-6}$ 1/ps)	Δ (10^{-6} 1/ps)
0.0	39.7	39.3	34.1	5.5
1.25	39.7	39.3	34.0	5.5
10.0	39.6	39.3	34.0	5.5
150.0	38.7	38.6	32.8	5.9
250.0	36.9	37.1	30.7	6.4

[a]Anisotropy (Δ) is calculated by combining the terms $3D^{rr} - D_{i=x,y,z}^{rr}$. Values for ρ = 0.0 mg/mL are derived based on the data given in Table 1.

We used the obtained values of Δ to fit the $\bar{C}_2(t)$ decays derived from the simulations (Figure 9), with double-exponential functions from eq 17, using only a single free parameter, namely D^{rr}. The accuracy of fitting was similar as in the case of $C_1^{i=x,y,z}(t)$ functions (we note that in the case of the most dense solution the root-mean-square error is several times smaller than the one resulting from monoexponential fits that are given in Table 2) and the resulting values of D^{rr} are given in Table 4. Finally, by combining terms $3D^{rr} - D_{i=x,y,z}^{rr}$ from Table 3 and values of D^{rr} from Table 4, we are able to determine all three eigenvalues of the HEWL's rotational diffusion tensors, D_x^{rr}, D_y^{rr}, D_z^{rr} (Table 4). Least affected by excluded volume interactions is the dynamics of rotations around the z axis of HEWL's PCS, described with the largest eigenvalue of the HEWL's rotational diffusion tensor—which is a consequence of the slightly elongated shape of HEWL (Figure 1, Table 1). Moreover, from the values of the ratio $(\Delta/D^{rr}) \times 100\%$ obtained for different densities of HEWL solutions, one can conclude that the apparent anisotropy of HEWL's rotational dynamics increases with the increasing influence of steric interactions, from 29% for the most dilute solution up to 36% for the most dense solution studied here.

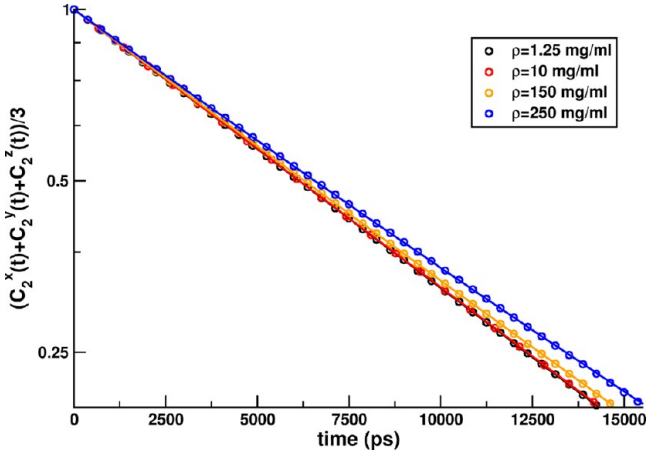

Figure 9. Rotational correlation functions $\bar{C}_2(t)$ derived from BD simulations of monodisperse solutions of HEWL molecules of different densities (cicrcles) and fits of double-exponential curves (continuous lines).

dx.doi.org/10.1021/ct4008519 | J. Chem. Theory Comput. 2014, 10, 481−491

Table 4. Average Diffusion Coefficients (D^r) of HEWL Resulting from Fitting of Double-Exponential Decays to Functions $\bar{C}_2(t) = {}^1/_3(C_2^x(t) + C_2^y(t) + C_2^z(t))$ Derived from BD Trajectories of Differently Concentrated HEWL Solutions[a] 1

ρ (mg/mL)	D^r (10^{-6} 1/ps)	D_x^r(10^{-6} 1/ps)	D_y^r(10^{-6} 1/ps)	D_z^r(10^{-6} 1/ps)	$\Delta/D^r \times$ 100%
0.0	18.9	16.9	17.2	22.5	29
1.25	18.9	16.9	17.2	22.6	29
10.0	18.8	16.9	17.1	22.5	29
150.0	18.4	16.5	16.6	22.4	32
250.0	17.6	15.8	15.6	22.1	36

[a]See text for details. Eigenvalues of rotational diffusion tensors, $D_{i=x,y,z}^r$, are computed based on the obtained values of D^r and terms $3D^r - D_{i=x,y,z}^r$ from Table 3. Values for ρ = 0.0 mg/mL are derived based on the data given in Table 1.

4. CONCLUSIONS

In analyses of trajectories of molecular systems generated using available computational techniques,[5,26−33] evaluation of rotational correlation functions defined for particular vectors attached to the simulated molecule presents a natural and a convenient way to investigate the rotational dynamics of molecules. Data resulting from computer simulations can be related directly to experimental observations of the rotational dynamics of molecules by evaluating rotational correlation functions based on the first and the second Legendre polynomials. Usually, the most interesting subjects of physical, chemical, or biological studies involve molecules of arbitrary shape, and it is crucial to employ in such studies models and tools that are valid in case of molecular objects that do not possess elements of symmetry. We have shown that hydrodynamic anisotropies of aspherical molecules should be explicitly taken into account in rigid-body BD simulations to properly describe their rotational dynamics, particularly, when excluded volume interactions come into play. The difference between the values of the HEWL's average rotational diffusion coefficient obtained from the BD simulation that takes into account hydrodynamic anisotropy of the proteins and from the BD simulation in which HEWLs are treated as hydrodynamically isotropic objects is within 2% (Tables 2 and 4). While such a difference can be considered negligible, it is statistically significant, and for biomolecules with anisotropies larger than that of HEWL, such differences would be more pronounced. Moreover, rigid-body BD simulations that employ fully anisotropic diffusion tensors of proteins allow one to evaluate not only the average rotational diffusion coefficient but also the eigenvalues of effective rotational diffusion tensors. Taking monodisperse HEWL solutions of varying density as our model system, we could see how these eigenvalues change with the increasing concentration of protein crowders. The rotational diffusion coefficients derived from such BD simulations have sound physical meaning. What is more important, we were able to observe a 25% increase in the apparent anisotropy of HEWL upon changing the concentration of the simulated solution from 0 mg/mL (infinite dilution limit) to 250 mg/mL (Table 4), an effect that is potentially of biological importance, that could not be observed with an isotropic description of simulated molecules.

While in the work described here we considered only excluded volume interactions between diffusing objects, the immediate extension of the presented subject that we are considering currently is a systematic study on molecular systems with long-range interactions of electrostatic nature. Such interactions between dissolved molecules are a source of local fields that influence their rotational dynamics. For example, it has been concluded, based on the solution of the rotational Smoluchowski equation,[61] that anisotropic electrostatic interactions appreciably influence the orientational relaxation of linear molecules. The extent to which the influence of electrostatics modifies rotational dynamics of molecules, or even the validity of the free diffusion model (that as we described above is strictly applicable only for an ensemble of independent Brownian particles) in case of long-range interactions acting between particles, can be investigated using rigid-body Brownian dynamics simulations.

Another factor that should be taken into account are solvent-mediated hydrodynamic interactions that introduce correlations between diffusing objects. Their influence is particularly difficult to address in case of arbitrarily shaped molecules, due to their long-range, many-body character prevalent at small intermolecular separations, and an appreciable computational cost associated with their evaluation. However, some insights can be gained from simulations of dilute solutions of simple anisotropic model molecules, within the framework of the far-field, two-body approximation of hydrodynamic interactions.

While in our studies we used the rigid-body Brownian dynamics technique, we note that, in general, the analysis that we have performed can also be applied to results of molecular dynamics simulations with their force fields and their different solvent treatments, to evaluate diffusion tensors and diffusion coefficients of simulated molecules.

■ ASSOCIATED CONTENT

Ⓢ Supporting Information

Expressions for first- and second-rank rotational correlation functions of an unitary vector attached to a freely diffusing rigid body. This material is available free of charge via the Internet at http://pubs.acs.org.

■ AUTHOR INFORMATION

Corresponding Author

*E-mail: mdlugosz@cent.uw.edu.pl. Phone: +48 22 5540 821. Fax: +48 22 5540 801.

Notes

The authors declare no competing financial interest.

■ ACKNOWLEDGMENTS

The authors acknowledge support from National Science Centre (N N519 646640). This research was supported in part by PL-Grid Infrastructure (ACK Cyfronet AGH).

■ REFERENCES

(1) Cukier, R. I. *J. Chem. Phys.* **1974**, *60*, 734−743.
(2) Alessi, L.; Andreozzi, L.; Faetti, M.; Leporini, D. *J. Chem. Phys.* **2001**, *114*, 3631−3639.
(3) Ermak, D. L.; J. A. McCammon, J. A. *J. Chem. Phys.* **1978**, *69*, 1352−1360.
(4) Allison, S. *Macromolecules* **1991**, *24*, 530−536.
(5) Fernandes, M. X.; García de la Torre, J. *Biophys. J.* **2002**, *83*, 3039−3048.
(6) Tokmakoff, A. *J. Chem. Phys.* **1996**, *105*, 1−12.
(7) Thomas, J. C.; Schurr, J. M.; Hare, D. R. *Biochemistry* **1984**, *23*, 5407−5413.

(8) Burghardt, T. P.; Thompson, N. L. *Biochemistry* **1985**, *24*, 3731−3735.
(9) Chirico, G.; Collini, M.; Tóth, K.; Brun, N.; Langowski, J. *Eur. Biophys. J.* **2001**, *29*, 597−606.
(10) Bruno, A.; De Lisio, C.; Minutolo, P. *Opt. Express* **2005**, *13*, 5393−5408.
(11) Wegener, W. A.; Dowben, R. M.; Koester, V. J. *J. Chem. Phys.* **1979**, *70*, 622−632.
(12) Woessner, D. E. *J. Chem. Phys.* **1962**, *3*, 647−654.
(13) Déjardin, J. L.; Deblais, G.; Boulli, B.; Henri-Rousseau, O. *J. Mol. Liq.* **1994**, *62*, 83−92.
(14) Favro, L. D. *Phys. Rev.* **1960**, *119*, 53−62.
(15) Kalmykov, Y. P. *J. Chem. Phys.* **2009**, *130*, 134105.
(16) Belford, G. G.; Belford, R. L.; Weber, G. *Proc. Natl. Acad. Sci. U.S.A.* **1972**, *69*, 1392−1393.
(17) Perrin, F. *J. Phys. Radium* **1934**, *5*, 497−511.
(18) Perrin, F. *J. Phys. Radium* **1936**, *7*, 1−11.
(19) Ehrenberg, M.; Rigler, R. *Chem. Phys. Lett.* **1972**, *14*, 539−544.
(20) Chuang, T. J.; Eisenthal, K. B. *J. Chem. Phys.* **1972**, *57*, 5094−5097.
(21) Smith, P. E.; van Gunsteren, W. F. *J. Mol. Biol.* **1996**, *236*, 629−636.
(22) Hubbard, J. B.; Wolynes, P. G. *J. Chem. Phys.* **1978**, *69*, 998−1006.
(23) Pecora, R. *J. Chem. Phys.* **1968**, *49*, 1036−1043.
(24) Ehrenberg, M.; Rigler, R. *Chem. Phys.* **1974**, *4*, 390−401.
(25) Ehrenberg, M.; Rigler, R. *Q. Rev. Biophys.* **1976**, *9*, 69−81.
(26) Ravichandran, S.; Bagchi, B. *J. Chem. Phys.* **1999**, *111*, 7505−7511.
(27) Hu, C.; Fang, J.; Borchardt, R. T.; Schowen, R. L.; Kuczera, K. *Proteins: Struct. Funct. Bioinf.* **2008**, *71*, 131−143.
(28) Sun, X.; Lin, T.; Gezelter, J. D. *J. Chem. Phys.* **2008**, *128*, 234107.
(29) Bac, C. G.; Paredes, V. R.; Vásquez, R. C.; Medina, D. E.; Hasmy, A. *Phys. Rev. E* **2001**, *63*, 042701.
(30) Mereghetti, P.; Wade, R. C. *J. Phys. Chem. B* **2012**, *116*, 8523−8533.
(31) McGuffee, S. R.; Elcock, A. H. *PLoS Comput. Biol.* **2010**, *6*, e1000694.
(32) Frembgen-Kesner, T.; Elcock, A. H. *J. Chem. Theory Comput.* **2009**, *5*, 242−256.
(33) Balbo, J.; Mereghetti, P.; Herten, D.; Wade, R. C. *Biophys. J.* **2013**, *104*, 1576−1584.
(34) Gaab, K. M.; Bardeen, C. J. *Phys. Rev. Lett.* **2004**, *93*, 056001.
(35) Diamond, R. *J. Mol. Biol.* **1974**, *82*, 371−391.
(36) Humphrey, W.; Dalke, A.; Schulten, K. *J. Molec. Graphics* **1996**, *14*, 33−38.
(37) Elcock, A. H. *Proc. Natl. Acad. Sci. U.S.A.* **2003**, *100*, 2340−2344.
(38) Ando, T.; Skolnick, J. *Proc. Natl. Acad. Sci. U.S.A.* **2010**, *107*, 18457−18462.
(39) Roosen-Runge, F.; Hennig, M.; Zhang, F.; Jacobs, R. M. J.; Sztucki, M.; Schober, H.; Seydel, T.; Schreiber, F. *Proc. Natl. Acad. Sci. U.S.A.* **2011**, *108*, 11815−11820.
(40) Cichocki, B.; Hinsen, K. *Phys. Fluids* **1995**, *7*, 285−291.
(41) Długosz, M.; Antosiewicz, J. M. *J. Phys. Chem. B* **2013**, *117*, 6165−6174.
(42) Brenner, H. *J. Colloid. Sci.* **1965**, *20*, 104−122.
(43) Harvey, S. C.; García de la Torre, J. *Macromolecules* **1980**, *13*, 960−964.
(44) García Bernal, J. M.; García de la Torre, J. *Biopolymers* **1980**, *19*, 751−766.
(45) Carrasco, B.; García de la Torre, J. *Biophys. J.* **1999**, *76*, 3044−3057.
(46) García de la Torre, J.; Bernadó, P.; Pons, M. *Methods Enzymol.* **2005**, *394*, 419−430.
(47) García de la Torre, J. *Biophys. Chem.* **2001**, *94*, 265−274.
(48) Roy, D.; Patel, N.; Conte, S.; Maroncelli, M. *J. Phys. Chem.* **2010**, *114*, 8410−8424.
(49) García de la Torre, J.; Carrasco, B.; Harding, S. E. *Eur. Biophys. J.* **1997**, *25*, 361−372.
(50) García de la Torre, J.; Harding, S. E.; Carrasco, B. *Eur. Biophys. J.* **1999**, *28*, 119−132.
(51) Antosiewicz, J.; Porschke, D. *J. Phys. Chem.* **1989**, *93*, 5301−5305.
(52) Antosiewicz, J. *Biophys. J.* **1995**, *69*, 1344−1354.
(53) Długosz, M.; Zielinski, P.; Trylska, J. *J. Comput. Chem.* **2011**, *32*, 2734−2744.
(54) Długosz, M.; Antosiewicz, J. *J. Chem. Theory Comput.* **2013**, *9*, 1667−1677.
(55) Mereghetti, P.; Gabdoulline, R. R.; Wade, R. C. *Biophys. J.* **2010**, *99*, 3782−3791.
(56) McGuffee, S. R.; Elcock, A. H. *J. Am. Chem. Soc.* **2006**, *128*, 12098−110.
(57) Shim, Y.; Jeong, D.; Choi, M. Y.; Kim, H. J. *J. Chem. Phys.* **2006**, *125*, 061102.
(58) Wieczorek, G.; Zielenkiewicz, P. *Biophys. J.* **2008**, *95*, 5030−5036.
(59) Spaar, A.; Dammer, C.; Gabdoulline, R. R.; Wade, R.; Helms, V. *Biophys. J.* **2006**, *90*, 1913−1924.
(60) Schluttig, J.; Korn, C. B.; Schwarz, U. S. *Phys. Rev. E.* **2010**, *81*, 030902(R).
(61) Felderhof, B. U. *J. Chem. Phys.* **2002**, *117*, 3583−3596.